IOPscience iopscience.iop.org

Home Search Collections Journals About Contact us My IOPscience

The influence of chlorine ion on the spectroscopic properties of Nd^{3+}- and Eu^{3+}-doped fluorochloride glass

This article has been downloaded from IOPscience. Please scroll down to see the full text article.

1998 J. Phys.: Condens. Matter 10 4985

(http://iopscience.iop.org/0953-8984/10/23/007)

View the table of contents for this issue, or go to the journal homepage for more

Download details:
IP Address: 171.66.16.209
The article was downloaded on 14/05/2010 at 16:30

Please note that terms and conditions apply.

J. Phys.: Condens. Matter **10** (1998) 4985–5006. Printed in the UK PII: S0953-8984(98)88999-6

The influence of chlorine ion on the spectroscopic properties of Nd^{3+}- and Eu^{3+}-doped fluorochloride glass

J Fernández†, R Balda† and J L Adam‡

† Departamento de Física Aplicada I, Escuela Técnica Superior de Ingenieros Industriales y de Telecomunicación, Universidad del País Vasco, Alameda de Urquijo s/n 48013 Bilbao, Spain

‡ Laboratoire de Verres et Céramiques, Campus de Beaulieu, Université de Rennes I, 35042 Rennes Cédex, France

Received 4 November 1997, in final form 18 February 1998

Abstract. The influence of local coordination ions on the optical properties of Nd^{3+} and Eu^{3+} in fluorochloride glass has been investigated by using steady-state and time-resolved laser excited site selective spectroscopy. From the thermal behaviour of lifetimes of the $^4F_{3/2}$ state, a T^3 dependence for the nonradiative Nd–Nd relaxation process has been found in the 10–90 K temperature range for Nd^{3+} concentration higher than 0.5 mol% which is in agreement with a two-site nonresonant process. In spite of the high content of fluorine in this glass, the presence of chlorine anions causes a significant effect on the spectral behaviour and relative quantum efficiency of Nd^{3+} emission as compared with those of pure fluoride glasses. The excitation wavelength dependence of the lifetimes of the $^4F_{3/2}$ state points to the existence of some site segregation for Nd^{3+} in this fluorochloride glass. This result is also confirmed by fluorescence line-narrowing experiments performed with Eu^{3+} in the same glass. The behaviour of both the line-narrowed fluorescence of the $^5D_0 \rightarrow {}^7F_2$ hypersensitive transition and the linewidth of the time-resolved resonant line-narrowed $^5D_0 \rightarrow {}^7F_0$ emission band as a function of the selective $^7F_0 \rightarrow {}^5D_0$ excitation wavelength indicates that homogeneous linewidths are dominated by relaxation time broadening caused by rapid phonon relaxation processes. These results together with the crystal field strength calculated as a function of excitation energy along the $^7F_0 \rightarrow {}^5D_0$ absorption band might be interpreted as indicating the existence of a crossover between the behaviour of fluorinelike and chlorinelike coordination anions. A discussion on the origin of this behaviour is given.

1. Introduction

In the last two decades considerable progress has been made both in the discovery of new compositions for halide glasses and in the knowledge of their optical properties. The main interest of these materials is the possibility of extending the infrared (IR) transparency domain towards longer wavelengths and consequently of achieving mid-infrared ultratransparency. But besides the potential uses related to their passive optical behaviour, many other important applications arise when glasses are doped by rare-earth (RE) ions.

The optical properties of rare-earth ions in glasses depend on the chemical composition of the glass matrix, which determines the structure and nature of the bonds [1]. The development of new glass-based optical devices requires a better understanding of the interionic interactions which are deeply involved in the fundamental physics of rare-earth ions. Moreover, the increasing evidence of structural ordering in glasses [2] has determined a renewed search of new glass systems and experimental techniques which could help to

0953-8984/98/234985+22$19.50 © 1998 IOP Publishing Ltd

understand the variety of structural possibilities emerging from the delicate compromise imposed by the cation–anion framework and the coordination requirements.

Among the numerous halide glass compositions which have been described in the literature only a few have been deeply investigated because the study of their optical properties requires samples of a reasonable size, optical quality and good resistance to moisture corrosion. Most heavy metal fluoride based glasses fulfill these requirements and as a consequence have received increasing attention. In particular, because of their extended infrared transmission, a great effort to develop ultralow-loss optical fibres in the mid-infrared has been realized. On the other hand, their ability to incorporate significant amounts of RE ions, and their high emission efficiency due to multiphonon emission rates which are lower than in other glasses, have made them attractive candidates for optical amplifiers and laser applications [3].

Besides heavy metal fluoride glasses, there are a number of heavy metal halide systems known to transmit further in the infrared than pure fluoride glasses. $ZnCl_2$ is the best glass former and the most widely known. Its infrared edge in the 12 to 13 μm region is of interest for optical operation in the 8 to 12 μm atmospheric window [4]. Although many attempts have been made to increase its resistance to water corrosion and to devitrification, hygroscopicity is still very high and affects the optical properties in the IR region. Cadmium chloride has also been proved to lead to vitreous materials [5]. When $CdCl_2$ glasses are stabilized by a mixture of chloride and fluoride such as CdF_2–BaF_2–NaCl, or others [6], the resistance to aqueous corrosion increases but the multiphonon edge is then determined by the metal fluoride bond and shifts to shorter wavelengths. Recently, fluorochloride glasses based on Cd, Na, Ba and Zn have been obtained which are stable and present lower phonon energies than those of conventional fluorozirconates or barium–indium–gallium fluoride glasses. The limit of infrared transparency in these fluorochloride glasses is around 9 μm, with a shift of 4 μm if compared to well known ZBLAN fluoride glasses [7]. Therefore high emission efficiencies can be expected for rare earths in these matrices.

Among the various rare-earth ions, neodymium is the most widely studied ion in a variety of glasses not only because of its applications, but also because the variations with composition of its spectroscopic properties usually apply to other trivalent rare-earth ions [8]. These properties include absorption and emission cross-sections, peak wavelengths and linewidths, lifetimes and quantum efficiencies and fluorescence quenching processes. To achieve the highest efficiency, fluorescence lifetimes of Nd^{3+} ions must closely approach the calculated radiative lifetime which is determined by all the competing radiative and nonradiative decay processes; the latter include both Nd–Nd self-quenching and multiphonon relaxation. Concentration quenching and multiphonon emission are dependent on the RE ion and the glass hosts [9]. On the other hand, europium ion is a well known luminescence probe for glass inhomogeneity [10, 11]. Since $^5D_0$ state is nondegenerate under any symmetry, the structure of the $^5D_0 \rightarrow {}^7F_J$ emission is only determined by the splitting of the terminal levels caused by the local crystal field. Moreover, as the $^7F_0$ level is also nondegenerate, site-selective excitation within the inhomogeneous broadened $^7F_0 \rightarrow {}^5D_0$ absorption band can be performed by using the fluorescence line narrowing (FLN) technique to evaluate the local environment around the rare-earth ions. Although there is a huge amount of work dealing with the problem of inhomogeneity in glasses based on FLN results, up to now no general trends have been attained which may allow us to interpret the great variety of experimental results in a consistent way. The most comprehensive studies have been achieved in glasses containing trivalent europium [12–22]. Some of them have shown the difficulty of correlating the details of the glass structure at rare-earth ion sites with the FLN spectra. In recent years a great effort has been made to investigate by

molecular dynamics (MD) the local structure around rare-earth ions embedded in glass matrices [10, 11]. More recent works on MD simulation of trivalent europium ion doped in silica and sodium disilicate [23, 24] allowed the authors to validate the proposed structural model and to investigate the spectra–structure correlations in these glasses. For this type of glass, the rare-earth environment seems to be composed of a continuous distribution of local-field sites and the authors conclude that the local structure of the europium ions is influenced to a greater degree by bonding and energetic requirements than by the silicate framework topology. On the other hand, recent results on the optical spectroscopy of Eu^{3+} in borosilicate glass [21] give evidence of two distinguishable distributions of sites for europium ions which the authors attribute to the silicate and borate portions of the glass network. Moreover, evidence of two non-equivalent sites in fluorozirconate [25] (ZBL) and in more complex heavy metal fluoride glasses have also been reported [20] by using site-selective spectroscopy. Experimental anomalies in the homogeneous linewidth found in Eu^{3+} doped fluoride glasses [26] were attributed to the possibility that active ions change from being modifiers to substituting network formers. In the case of fluorochloride glasses, as far as we know, the only MD simulation of an Eu^{3+} doped glass has been performed for the ZrF_4–BaF_2–EuF_3 systems in which the substitution of F^- by Cl^- was carried out up to 10% in total number of anions [27]. Although CNBZn glass has a different composition and the conclusions of this work cannot be directly applied to our system, if we take into account the relative similarities among the electronic structure and ionic radius of Cd^{2+} and Zr^{4+} ions plausible hypotheses concerning the local environment of Eu^{3+} in CNBZn glass can be drawn out from our investigation, as we shall see below.

The aim of this work is to study the influence of chlorine on the spectroscopic properties of Nd^{3+} and Eu^{3+} in fluorochloride glasses. The nature of the nonradiative Nd–Nd relaxation process and the influence of the mixed nearest-neighbour coordination on the Nd^{3+} emission is investigated. The study includes absorption and emission properties, lifetimes, fluorescence quenching processes and site-dependent effects. For a better understanding of the influence of the local coordination ions on the optical properties of RE ions in these mixed anion glasses we have analysed the optical properties of Eu^{3+} by making use of laser induced FLN spectroscopy. As we shall see, an appropriate combination of high resolution temporal and spectral FLN techniques can give an unequalled tool to study the structural ordering in glasses. The excitation wavelength dependence of lifetimes, homogeneous linewidths and average crystal field parameter can be interpreted as indicating the existence of a crossover between fluorinelike and chlorinelike rare-earth coordination ions. A discussion on the origin of this behaviour is also given.

2. Experiment

Fluorochloride glass samples were obtained with the molar composition $25CdF_2$–$13.5CdCl_2$–$30NaF$–$20BaF_2$–$1.5BaCl_2$–$10ZnF_2$. They are referred to as CNBZn in the text. Samples were prepared in a glove box under dry argon atmosphere from high purity starting materials. Glass transition, crystallization and melting temperatures are 169 °C, 241 °C and 367 °C, respectively. With a temperature difference of 72 °C between crystallization and glass transition, the glass is stable enough to obtain samples about 4 mm thick. As far as moisture sensitivity is concerned, the relatively low chlorine content makes these glasses more resistant than previous fluorochloride glasses [7]. The samples were doped with 0.1, 0.5 and 1 mol% of NdF_3, and 0.5 mol% of EuF_3. Finally the samples were cut and polished for optical measurements.

The sample temperature was varied between 4.2 and 300 K with a continuous flow cryostat. Conventional absorption spectra were performed with a CARY 5 spectrophotometer. The steady-state emission measurements were made with an argon laser as exciting light and the medium wave tuning range (800–920 nm) of a Ti–sapphire ring laser, pumped by an argon laser. The fluorescence was analysed with a 0.22 m SPEX monochromator, and the signal was detected by a Hamamatsu R7102 extended IR photomultiplier and finally amplified by a standard lock-in technique.

Lifetime measurements were performed with a tunable dye laser of 9 ns pulse width and 0.08 cm^{-1} linewidth. The time resolved emission measurements were obtained by exciting the samples with a Ti–sapphire laser, pumped by a pulsed frequency doubled Nd:YAG laser (9 ns pulse width), and detecting the emission with a Hamamatsu R7102 photomultiplier. Data were processed by a EGG-PAR boxcar integrator.

The $^5D_0 \rightarrow {}^7F_0$ transition of Eu^{3+} was excited by a pulsed frequency doubled Nd:YAG pumped tunable dye laser of 9 ns pulse width and 0.08 cm^{-1} linewidth. The time-resolved fluorescence was analysed and detected with a EGG-PAR optical multichannel analyser.

3. Spectroscopic results

3.1. Absorption properties

The room temperature absorption spectra of Nd^{3+}-doped fluorochloride glasses were recorded in the 300–2500 nm spectral range using a Cary 5 spectrophotometer. The spectral resolution was 0.5 nm at wavelengths below 1100 nm, and 2 nm above. As an example figure 1 shows the spectrum for CNBZn glass doped with 1 mol% of Nd^{3+} in the 300–900 nm range.

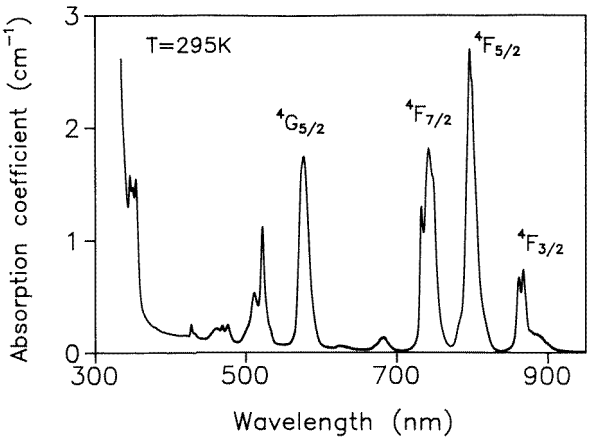

Figure 1. Room temperature absorption spectrum of Nd^{3+} (1 mol%) ions in fluorochloride glass.

The line strength of the electric-dipole transition between J states in the Judd–Ofelt [28, 29] treatment is given by [30]:

$$S = \sum_{t=2,4,6} \Omega_t |\langle (S', L')J' \| U^{(t)} \| (S, L)J \rangle|^2 \tag{1}$$

where Ω_t are the Judd–Ofelt intensity parameters (JO) and the $\langle \| U^t \| \rangle$ are the doubly

reduced unit tensor operators calculated in the intermediate coupling approximation [28]. Ten absorption bands lying between 427 and 2500 nm were integrated, and these data together with the value for the Nd^{3+} concentration and the refractive index were fitted by a computerized least squares program to yield the best fit values for the Judd–Ofelt parameters Ω_2, Ω_4, Ω_6 [28, 29]. It is known that the reduced matrix elements $\|U^t\|^2$ are almost independent of the ion environment. To estimate the Ω_t parameters we have used the values reported by W T Carnall *et al* [31] for Nd^{3+} ions in LaF_3. The JO parameters obtained for CNBZn glass are displayed in table 1, which also includes the values obtained in three pure fluoride glasses [32] for comparison. The root-mean-square deviation was around 25×10^{-8} in all glasses. These parameters are in good agreement with those previously reported for the Nd^{3+} ion in different glass materials [33–38]. As expected, the presence of chlorine anions results in higher values for the JO parameters [38].

Table 1. Judd–Ofelt parameters (10^{-20} cm^2) calculated from the absorption spectra of Nd^{3+} (1 mol%).

Glass	Ω_2	Ω_4	Ω_6
CNBZn	2.81	4.62	5.22
PZG[a]	1.53	3.19	4.93
ZBLAN[b]	2.66	3.05	4.08
BIGaZYTZr[c]	1.31	2.71	4.01

[a] $38PbF_2$–$20ZnF_2$–$35GaF_3$–$2InF_3$–$2CdF_2$–$3LaF_3$.
[b] $58ZrF_4$–$18BaF_2$–$5.5LaF_3$–$3AlF_3$–15NaF.
[c] $30BaF_2$–$18InF_3$–$20ZnF_2$–$10YF_3$–$6ThF_4$–$12GaF_3$–$4ZrF_4$.

3.2. Emission properties

The $^4F_{3/2} \rightarrow {}^4I_{11/2}$ steady-state fluorescence spectra at room temperature were measured by exciting the samples with an argon laser. Figure 2 shows this emission spectrum for CNBZn glass doped with 1 mol% of Nd^{3+}. The emission is inhomogeneously broadened due to site-to-site variations in the local ligand field. The fluorescence band was integrated and divided by the peak intensity to yield an effective linewidth [30]. The stimulated emission cross-section can be determined from spectral parameters by making use of [30]:

$$\sigma_p(\lambda_p) = \frac{\lambda_p^4}{8\pi c n^2 \Delta\lambda_{eff}} A[(^4F_{3/2}); (^4I_{11/2})] \tag{2}$$

where λ_p is the peak fluorescence wavelength, n is the refractive index, $\Delta\lambda_{eff}$ is the effective linewidth of the transition and $A[(^4F_{3/2}); (^4I_{11/2})]$ is the radiative transition probability for this transition.

The spontaneous emission probabilities from the $^4F_{3/2}$ to the ^4I_J states can be calculated from the JO parameters. The radiative transition probability from the initial J' manifold $|(S', L')J'\rangle$ to the terminal manifold $|(S, L)J\rangle$ is given by [30]:

$$A[(S', L')J'; (S, L)J] = \frac{64\pi^4 e^2}{3h(2J'+1)\lambda^3} n \left[\frac{(n^2+2)^2}{9}\right] \times \sum_{t=2,4,6} \Omega_t |\langle (S', L')J' \| U^{(t)} \| (S, L)J \rangle|^2 \tag{3}$$

where $n(n^2+2)^2/9$ is the local field correction for the Nd^{3+} ion in the initial J' manifold, n is the refractive index, λ is the wavelength of the transition and J is the terminal manifold.

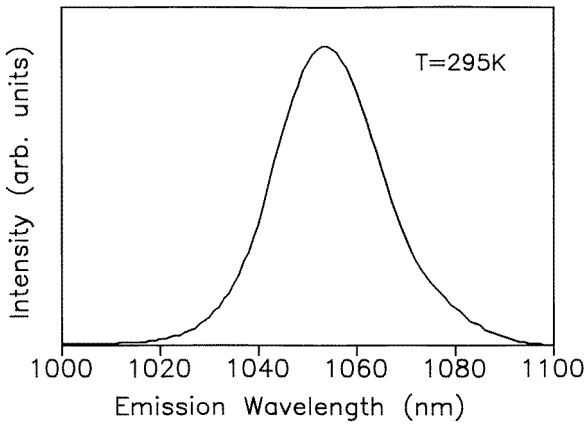

Figure 2. Room temperature fluorescence spectrum of the $^4F_{3/2} \rightarrow {}^4I_{11/2}$ transition of Nd^{3+} (1 mol%) in fluorochloride glass obtained under excitation with an argon laser.

The radiative lifetime of the $^4F_{3/2}$ state can be calculated from:

$$\tau_R = \sum_J A[(^4F_{3/2}); (^4I_J)]. \tag{4}$$

The branching ratios can be obtained from the transition probabilities by using [30]:

$$\beta(^4F_{3/2}; {}^4I_J) = \frac{A[(^4F_{3/2}); (^4I_J)]}{\sum_J A[(^4F_{3/2}); (^4I_J)]}. \tag{5}$$

These values together with the total spontaneous emission probability (W_R) are listed in table 2. This table also includes the data for three pure fluoride glasses. The fluorescence branching ratios from the $^4F_{3/2}$ state depend upon the ratio of Ω_4 and Ω_6 [33]. In this case, the highest value for the Ω_4 parameter corresponds to the fluorochloride glass, and therefore this glass presents the largest transition probability to the $^4I_{9/2}$ state.

Table 2. Branching ratios and spontaneous emission probability (W_R) for the $^4F_{3/2} \rightarrow {}^4I_J$ ($J = 9/2,\ 11/2,\ 13/2,\ 15/2$) transitions of Nd^{3+} (1 mol%) in fluorochloride glass and in pure fluoride glasses, obtained from the Judd–Ofelt parameters.

$^4F_{3/2} \rightarrow$	$^4I_{9/2}$	$^4I_{11/2}$	$^4I_{13/2}$	$^4I_{15/2}$	W_R (s^{-1})
CNBZn	0.416	0.4860	0.0931	0.0048	2942
PZG	0.361	0.525	0.1073	0.0056	2660
ZBLAN	0.391	0.504	0.100	0.0050	2002
BIGaZYTZr	0.379	0.511	0.105	0.0050	1767

The resulting radiative lifetime τ_R and the stimulated emission cross-section for the $^4F_{3/2} \rightarrow {}^4I_{11/2}$ transition are presented in table 3 together with the effective fluorescence linewidth. As can be seen, although the JO parameters for Nd^{3+} in the fluorochloride glass are slightly larger than in pure fluoride glasses, this glass presents the narrowest effective linewidth and the largest value for the stimulated emission cross-section.

Table 3. Room temperature emission properties of Nd^{3+} (1 mol%) in fluorochloride glass and in pure fluoride glasses. The radiative lifetime of the $^4F_{3/2}$ state has been estimated by using the Judd–Ofelt parameters.

Glass	n	$\Delta\lambda_{eff}$ (nm)	σ_p (10^{-20} cm^2)	τ_R (μs)	τ_{exp} (μs)
CNBZn	1.55	23.43	4.2	340	285
PZG	1.59	25.26	3.5	375	296
ZBLAN	1.51	23.85	2.9	499	430
BIGaZYTZr	1.54	25.15	2.7	537	409

3.3. Lifetime results

The decays of the $^4F_{3/2} \rightarrow {}^4I_{11/2}$ transition were performed with a narrow band (0.08 cm^{-1} linewidth) tunable dye laser of 9 ns pulse width, by exciting the samples at the $^4I_{9/2} \rightarrow {}^4G_{5/2}$ absorption band (575 nm). They were found to be single exponential at all temperatures and concentrations. As an example, figure 3 shows the room temperature logarithmic plot of the experimental decay for CNBZn glass, 1 mol% Nd^{3+}.

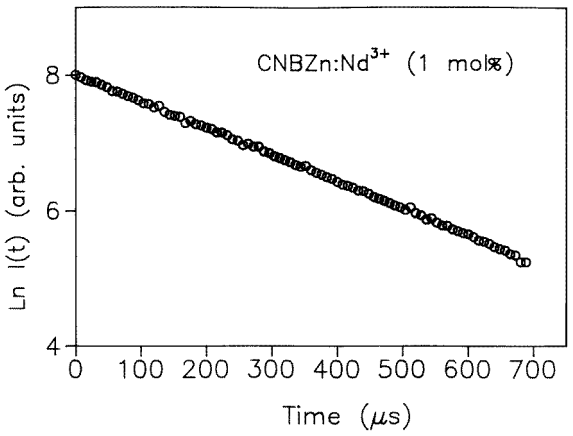

Figure 3. Logarithmic plot of the fluorescence decays of the $^4F_{3/2}$ state for the fluorochloride glass doped with 1 mol% of Nd^{3+}. The decays were obtained by exciting at the $^4I_{9/2} \rightarrow {}^4G_{5/2}$ absorption band and monitored at 1050 nm. Data correspond to 295 K.

The temperature dependences of the lifetimes were obtained in the 4.2–300 K temperature range for three different concentrations, 0.1, 0.5 and 1 mol% of Nd^{3+} in CNBZn glass. Figure 4 shows the lifetime values as a function of temperature.

The fluorescence decays for the $^4F_{3/2} \rightarrow {}^4I_{11/2}$ emission were also measured as a function of the excitation wavelength along the $^4I_{9/2} \rightarrow {}^4G_{5/2}$ absorption band at 77 K. Figure 5 shows that the lifetime (which remains single exponential) displays a variation of about 15% and does not show a monotonic variation with wavelength as should correspond to the case of only one kind of statistical site distribution for Nd^{3+} ions.

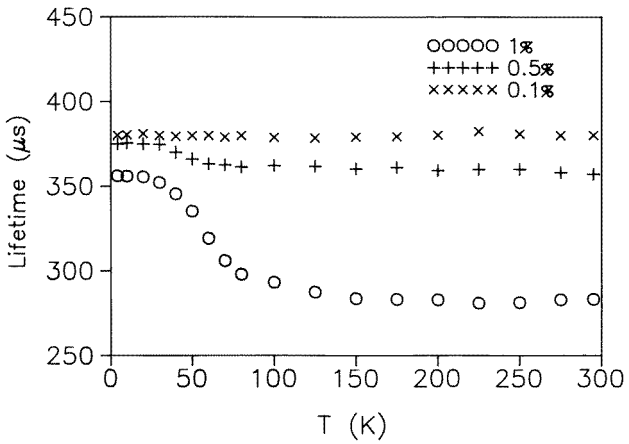

Figure 4. Temperature dependence of the $^4F_{3/2}$ state lifetime of Nd^{3+} ions in fluorochloride glass. (×) 0.1 mol%, (+) 0.5 mol% and (○) 1 mol%. Lifetimes were obtained by exciting at 575 nm and collecting the fluorescence at the emission peak of the $^4F_{3/2} \rightarrow {}^4I_{11/2}$ transition.

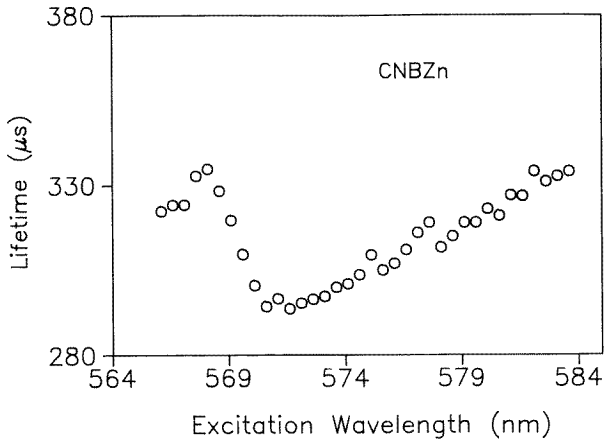

Figure 5. Lifetimes of the $^4F_{3/2}$ state as a function of excitation wavelength along the $^4I_{9/2} \rightarrow {}^4G_{5/2}$ absorption band for CNBZn glass doped with 1 mol% of Nd^{3+}. Lifetimes were obtained at 77 K collecting the fluorescence at the emission peak of the $^4F_{3/2} \rightarrow {}^4I_{11/2}$ transition.

4. Discussion

4.1. Nd^{3+}–Nd^{3+} energy transfer and luminescence quantum efficiency

As can be seen in figure 4, as concentration rises the experimental lifetime decreases even at helium temperature, indicating that Nd–Nd relaxation processes are present at concentrations higher than 0.5 mol%. This thermal behaviour also suggests the presence of quite a strong thermal mechanism between 10 K and 100 K at concentrations higher than 0.5 mol%. It is well known that the Nd^{3+} fluorescence quenching depends on glass composition [9]. In a previous work [32] some of the present authors have investigated the temperature dependent concentration quenching of Nd^{3+} fluorescence in three pure fluoride glasses which shows

a strong thermal quenching between 10 K and 90 K where the nonradiative rates were found to increase with temperature as T^3. This is in agreement with a two-site nonresonant process in the short-wavelength regime as has been shown by Holstein *et al* [39]. In this process, the phonon emission and absorption take place at different sites, the ion–phonon interaction acts twice and the site–site Hamiltonian once. This phonon-assisted excitation transfer between different states of similar ions could be understood by considering a small spread in the energy values of $^4F_{3/2}$ transitions to the J multiplicity, due to the inherent disorder of the glass structure.

For comparison, figure 6 shows the thermal behaviour of Nd^{3+} lifetime in three fluoride glasses and in the investigated fluorochloride glass for the same concentration ($\approx 2.2 \times 10^{20}$ ions cm^{-3}). As can be seen lifetime decreases between 4.2 K and 100 K in all cases.

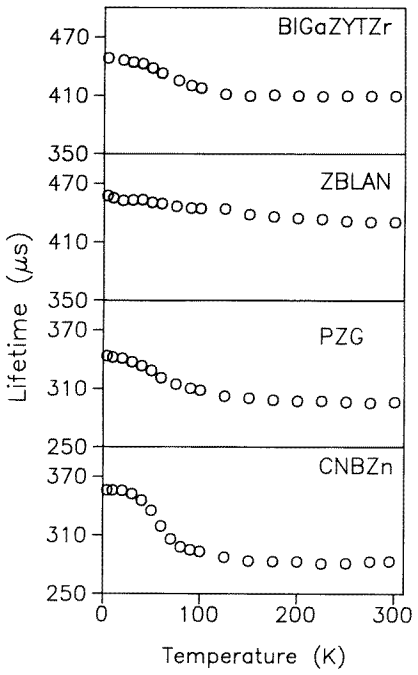

Figure 6. Lifetimes as a function of temperature for Nd^{3+} ions ($\approx 2 \times 10^{20}$ cm^{-3}) in three pure fluoride glasses and in CNBZn glass. Lifetimes were obtained by exciting at 575 nm and collecting the luminescence at the emission peak of the $^4F_{3/2} \rightarrow {}^4I_{11/2}$ transition.

The lifetime of the $^4F_{3/2}$ state of Nd^{3+} ion in the doped glasses should be governed by the sum of probabilities for several competing processes such as radiative decay, nonradiative decay by multiphonon emission and energy transfer to other Nd^{3+} ions. In this case the multiphonon relaxation rate for the $^4F_{3/2}$ state is expected to be small because of the high energy gap to the next lower-lying J manifold (≈ 5500 cm^{-1}) and the typical values of phonon energies involved ($\leqslant 450$ cm^{-1}). If one assumes that the purely radiative lifetimes τ_R of $^4F_{3/2}$ levels are independent of Nd^{3+} concentration and temperature, and disregards multiphonon relaxation processes, the variations of the experimental lifetimes can be related

to the nonradiative Nd–Nd relaxation processes by the simple relation:

$$\tau_{exp}^{-1} = \tau_R^{-1} + W_{Nd-Nd}(T) \tag{6}$$

where τ_{exp} is the measured lifetime and τ_R represents the radiative lifetime.

If we disregard the multiphonon relaxation processes, relaxation via fast Nd–Nd diffusion processes and subsequent deexcitation via energy sinks should be taken into account, as they occur even at low temperatures. Figure 7 shows the plot of $[W_{Nd-Nd}(T) - W_{Nd-Nd}(0)]^{1/3}$ in the 10–90 K range for CNBZn glass and for three pure fluoride glasses doped with 1 mol% of Nd^{3+}. It is worth noticing the good fit of the Nd–Nd relaxation probability to a T^3 dependence in all cases, indicating that the same mechanism for nonradiative processes is present in these glasses. In contrast, a recent investigation on fluorophosphate glasses with a high content of fluoride ions failed to show the same temperature dependence [40].

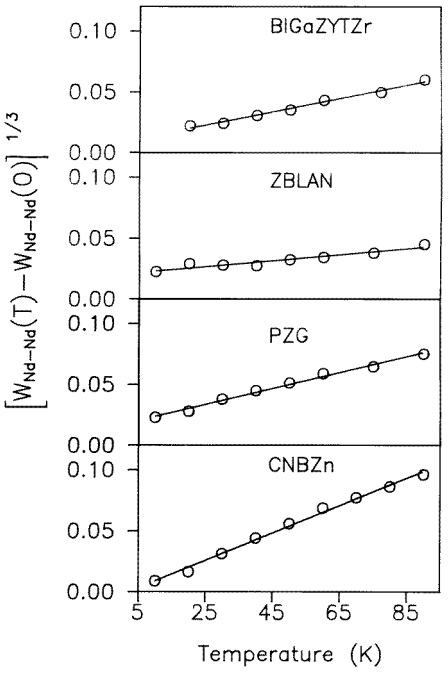

Figure 7. Plot of the non-radiative Nd–Nd relaxation rate in the 10–90 K temperature range for the fluorochloride glass and for three fluoride glasses doped with 1 mol% of Nd^{3+}. Symbols represent the experimental values, and solid lines are the fit to a T^3 dependence.

In order to compare the efficiency of the emission in fluorochloride glass and in fluoride glasses Nd^{3+} emission measurements were performed in such a way that an absolute comparison could be made among different glasses. The following procedure was used [41]. The fluorescence of all samples was excited by using the 514 nm line of a power stabilized argon laser. The samples were thin slabs cut and polished to have exactly the same thickness. The pumping radiation was focused into the sample using a microscope stage with a 0.25 m monochromator and a photomultiplier at the tube end. A low-magnifying objective was used for a close approximation to the upper surface of the sample. To avoid the direct entrance of pumping light on the monochromator, appropriate filters were used. Moreover, the Bertrand lens of the polarizing microscope was also used to slightly misalign

the path of the remaining pumping light reaching the entrance slit of the monochromator. The sample was placed so that the spectrometer collected all the luminescence coming from the sample volume contained within the solid angle subtended by the microscope objective. The relative quantum efficiency is taken as the integrated emission intensity of the $^4F_{3/2} \rightarrow {}^4I_{11/2}$ transition, normalized to the maximum value as unity. As can be seen in table 4, the CNBZn glass shows the highest luminescence efficiency.

Table 4. Relative quantum efficiency of Nd^{3+} (1 mol%) in fluorochloride glass and in the three pure fluoride glasses normalized to the maximum value as unity.

Glass	Relative quantum efficiency
CNBZn	1
PZG	0.73
ZBLAN	0.76
BIGaZYTZr	0.80

4.2. Site-dependent effects

4.2.1. Nd^{3+} sites. The optical properties of rare-earth doped glasses are closely related to the local structure and bonding at the ions site [8]. Although rare earths are not randomly distributed throughout the glass and they may or may not enter as former ions, their optical spectra show, even at low concentrations, an inhomogeneous broadening which is the evidence of large site-to-site crystal field variations. The presence of more than one type of anion inserts an additional complexity into the usual structural disorder inherent in a glass. Since this disorder plays an important role in the optical and laser properties of the Nd^{3+} ions, steady-state and time-resolved site-selective fluorescence measurements were performed to obtain information about the site distribution of Nd^{3+} ions and the energy transfer between them.

The site-selective fluorescence measurements were performed by exciting the $^4I_{9/2} \rightarrow {}^4F_{3/2}$ transition. Figure 8(a) shows the 4.2 K steady-state excitation spectra of Nd^{3+} ions corresponding to the transitions from the lower Stark component of the $^4I_{9/2}$ ground state to the $^4F_{3/2}$ state for CNBZn glass doped with 1 mol% of Nd^{3+}. The luminescence was collected at different wavelengths along the $^4F_{3/2} \rightarrow {}^4I_{11/2}$ emission. As can be observed at all emission wavelengths, instead of the two expected peaks corresponding to the $^4I_{9/2} \rightarrow {}^4F_{3/2}$ transition, the low energy component shows a complex structure, which points to the existence of at least two distinguishable site distributions for Nd^{3+} ions in this glass. The monochromatic radiation excites an isochromat corresponding to a subset of sites which may not necessarily be physically identical. Therefore, the emission line profile is a set of emissions from the two statistical site distributions which may have different natural homogeneous linewidths. As can be also observed in figure 8(a), the features shown by the excitation spectra are wavelength dependent but do not show any change with temperature. As wavelength increases the spectra become slightly broadened, corresponding to the contribution of a larger subset of Nd^{3+} sites.

The steady-state emission spectra for the $^4F_{3/2} \rightarrow {}^4I_{11/2}$ transition were recorded by exciting at different wavelengths in the low energy component of the $^4I_{9/2} \rightarrow {}^4F_{3/2}$ absorption band. Figure 8(b) shows the spectra at 4.2 K at different excitation wavelengths. As can be observed, under excitation at the high energy wing of the low energy Stark component of the $^4I_{9/2} \rightarrow {}^4F_{3/2}$ transition, the emission band shows two main peaks.

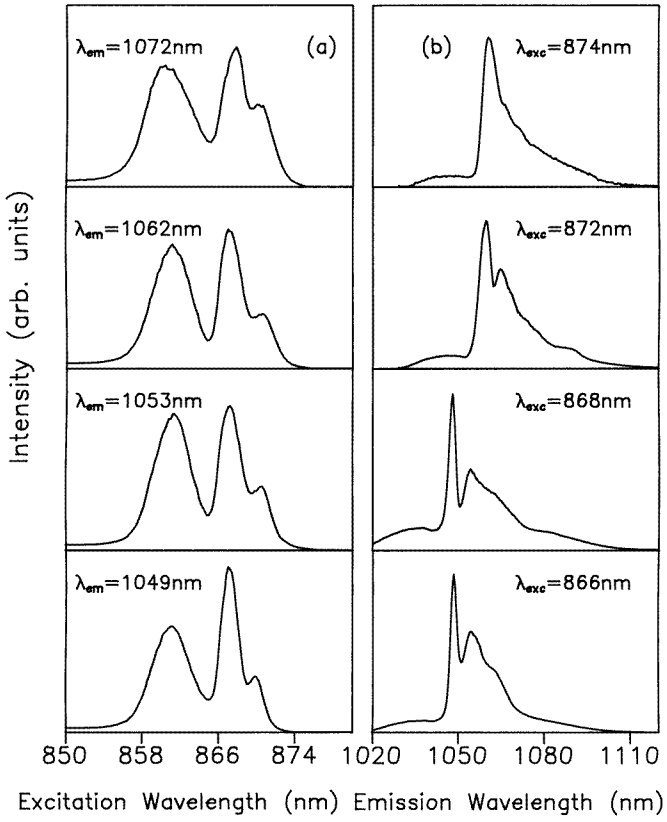

Figure 8. (a) Steady-state excitation spectra of $^4I_{9/2} \rightarrow {}^4F_{3/2}$ transition for luminescence monitored at different wavelengths within the $^4F_{3/2} \rightarrow {}^4I_{11/2}$ emission band and (b) steady-state emission spectra of $^4F_{3/2} \rightarrow {}^4I_{11/2}$ transition in CNBZn glass doped with 1 mol% of Nd^{3+} for different excitation wavelengths along the low energy Stark component of the $^4F_{3/2}$ level. Measurements were performed at 4.2 K.

However, as excitation goes to lower energies, the shape of the emission band evolves to a unique broad red-shifted peak which is due to the emission of the Nd^{3+} ions situated in low field sites.

The existence of energy transfer between Nd^{3+} ions in CNBZn glass has been demonstrated by using time-resolved spectroscopy. Time-resolved site-selective emission spectra for the $^4F_{3/2} \rightarrow {}^4I_{11/2}$ transition were performed at 77 K by exciting the samples into the $^4I_{9/2} \rightarrow {}^4F_{3/2}$ absorption band and recording the spectra at different time delays after the laser pulse. Figure 9 shows the time evolution of the $^4F_{3/2} \rightarrow {}^4I_{11/2}$ emission obtained by exciting at 860 nm and at two different time delays after the laser pulse. As can be observed, as time increases the spectrum narrows and shifts to the red showing the existence of energy transfer between Nd^{3+} ions. If energy transfer between ions in spectral different sites is present, energy migrates towards the lower energy sites giving a red shift in the emission. However, the transfer is fast enough to give exponential fluorescence decays [42].

Although remarkable site-effects have been reported by the authors on the spontaneous emission of Cr^{3+}-doped fluoride glasses [43–45], and on the stimulated emission of Nd^{3+} in

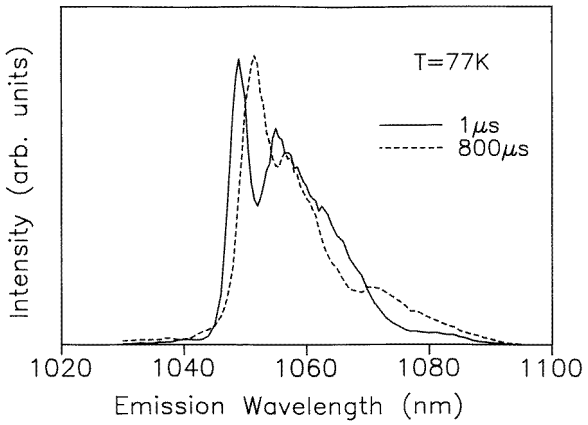

Figure 9. Time-resolved emission spectra of $^4F_{3/2} \rightarrow {}^4I_{11/2}$ transition in CNBZn glass doped with 1 mol% of Nd^{3+} obtained at two different time delays after the laser pulse by exciting at 860 nm. Measurements were performed at 77 K.

the same family of glasses, where more than one site distribution for Nd^{3+} ions were found [46, 47], in the case of CNBZn these site-effects could be even more important. In spite of the high fluoride content of CNBZn glass, the spectral behaviour of Nd^{3+} ions in this matrix is far from the one exhibited in pure fluoride glasses. Figures 10 and 11 show for comparison the different features of the excitation and emission spectra of Nd^{3+} corresponding to the $^4I_{9/2} \rightarrow {}^4F_{3/2}$ and $^4F_{3/2} \rightarrow {}^4I_{11/2}$ transitions respectively. It is worthwhile mentioning the sharper features presented by CNBZn glass, which are presumably related to the presence of chlorine in the Nd^{3+} environment and can be explained in the following way. The setting of the Nd^{3+} coordination, which occurs during the glass formation, is driven by the free energy of the rare-earth–anion polyhedron. The higher electronegativity of fluorine together with its smaller atomic radius favour its bonding with the smaller cations which constitute the network formers. On the other hand, chlorine, with a larger atomic radius, may advantageously substitute fluorine anions at network positions occupied by the larger cations which may be network former and/or modifiers. As a consequence, in the network glass forming process some exchange from fluorine to chlorine ions can be expected in this CNBZn glass which will greatly affect the local environment at the rare earth site and, therefore, will influence the radiative transition rates as electric dipolar transitions are sensitive to local symmetry changes. The wavelength dependence of the features observed in the low temperature emission and excitation spectra and lifetimes (section 3.3), together with those appearing in the time-resolved emission spectrum (spectral narrowing and change of shape), may suggest that this behaviour is related to the existence of some site segregation for neodymium in this fluorochloride glass, which might be due to the different kinds of ion coordination.

4.2.2. Eu^{3+} sites. As we have seen above, the spectral features of Nd^{3+}-doped fluorochloride glasses point to the presence of some ordering in the local environment of the rare earth. In order to investigate the nature of this site segregation for Nd^{3+} ions in CNBZn glass, we have performed fluorescence line narrowing experiments with Eu^{3+} (0.5 mol%) in the same glass matrix. Although the local environment of Eu^{3+} may be altered with respect to the Nd^{3+}-doped glass and therefore its value as a probe of intrinsic

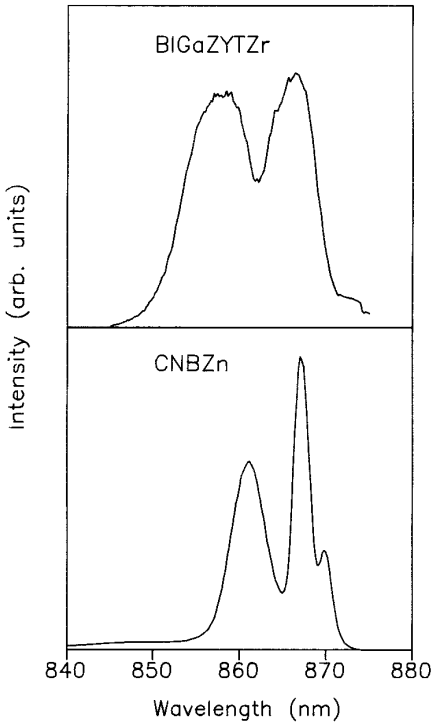

Figure 10. Steady-state excitation spectra of $^4I_{9/2} \rightarrow {}^4F_{3/2}$ transition in CNBZn and BIGaZYTZr glasses doped with 1 mol% of Nd^{3+} for luminescence monitored at 1049 nm. Measurements were performed at 4.2 K.

glass structure could be compromised, the comparison with the line-narrowed spectra of CNBZn glass with their counterpart in a pure fluoride glass will provide further insight into the nature and distribution of the local coordination ions in this fluorochloride glass.

It is well known that the $^5D_0 \leftrightarrow {}^7F_0$ transition of Eu^{3+} is ideally suited for an investigation of line broadening in glasses because a single transition between nondegenerate levels can be studied with no overlapping from neighbouring crystal field components. Moreover, the energy gap between $^5D_0$ state and the next lower $^7F_6$ state is about ten times the highest involved phonon energy. Therefore, the probability of non-radiative deexcitation of the $^5D_0$ state by multiphonon processes is very small. At low dopant concentrations (less than 1 mol%) and temperatures (4.2 K), cross relaxation via ion–ion interaction can be disregarded and the measured lifetimes of the $^5D_0$ state can be considered mainly radiative. Thus their dependence on excitation wavelength should parallel the variations of the electric dipolar transition rates [15]. On the other hand, ions in different environments have different electron–phonon coupling strengths and therefore will have different homogeneous linewidths. Because homogeneous linewidth, $\Delta\nu$, and relaxation (or dephasing) time τ are related by the expression $\Delta\nu = (2\pi\tau)^{-1}$, complementary information can be obtained by working either in the frequency or in the time domain [48].

Figure 12(a) shows the results obtained for the decay of the line-narrowed fluorescence of the $^5D_0 \rightarrow {}^7F_2$ hypersensitive transition of Eu^{3+} which is very sensitive to small changes in the chemical surroundings of the ion [49]. As can be observed, the dependence on excitation wavelength (by exciting along the $^7F_0 \rightarrow {}^5D_0$ absorption band) of the Eu^{3+}

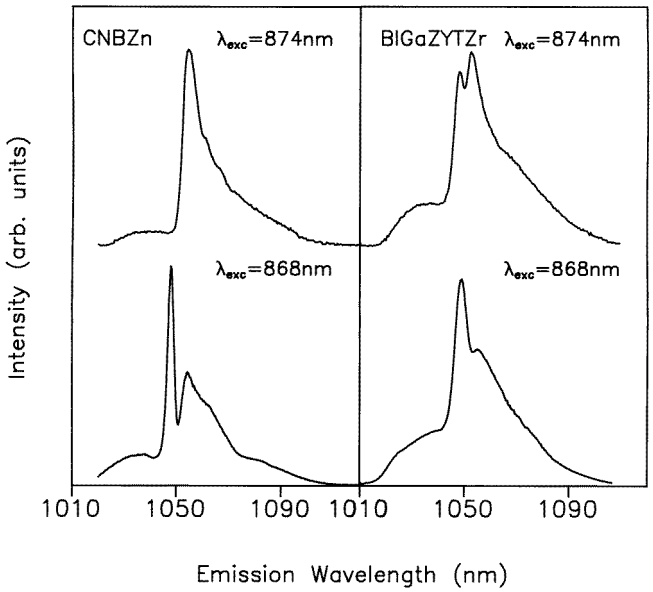

Figure 11. Steady-state emission spectra of $^4F_{3/2} \rightarrow {}^4I_{11/2}$ transition in CNBZn and BIGaZYTZr glasses doped with 1 mol% of Nd^{3+} for different excitation wavelengths along the low energy Stark component of the $^4F_{3/2}$ level. Measurements were performed at 4.2 K.

lifetime presents similar features (see figure 5) to the fluorescence decay for the $^4F_{3/2} \rightarrow {}^4I_{11/2}$ emission of Nd^{3+} as a function of the excitation wavelength along the hypersensitive $^4I_{9/2} \rightarrow {}^4G_{5/2}$ transition as far as its nonmonotonic behaviour is concerned. As is well known [50] a larger transition probability of the $^5D_0 \rightarrow {}^7F_2$ hypersensitive transition may correspond to an increase of covalent bonding induced by the presence of chlorine in the nearest-neighbour coordination of the Eu^{3+} which not only changes the geometrical atomic arrangement but also the bonding strength. As shown in figure 12(b), this lifetime result is mirrored by the measured linewidth of the time-resolved resonant line-narrowed $^5D_0 \rightarrow {}^7F_0$ emission band of Eu^{3+} as a function of excitation wavelength along the $^7F_0 \rightarrow {}^5D_0$ absorption band, obtained at 4.2 K and 100 μs after the laser pulse on a sample doped with 0.5 mol% of Eu^{3+}. Although the spectral width of the laser pulse (0.08 cm^{-1}) is much narrower than the expected homogeneous linewidth we were limited by the spectral resolution (3 cm^{-1}) of the optical multichannel analyser. Nevertheless, as the results are good enough to be compared with lifetimes we made no deconvolution in the resulting spectra. It is clear that homogeneous linewidths are dominated by relaxation time broadening caused by rapid phonon relaxation processes and therefore also yield very valuable information about the strength of ion–phonon coupling in this glass matrix.

It is worthwile to mention that, in spite of the relatively low chlorine content of CNBZn glass, its influence on the optical properties of rare earths seems to be very important. The effect of the gradual incorporation of chlorine ions into the Eu^{3+} surroundings can be also pictured by comparing the time-resolved resonant line-narrowed $^5D_0 \rightarrow {}^7F_{0,1,2}$ emission spectra of CNBZn with those of a pure fluoride glass. Figure 13 shows for comparison the spectra of BIGaZYTZr and CNBZn glasses obtained at 4.2 K for the same excitation wavelengths. As we can see, the shapes of the spectra are quite similar at wavelengths up to 578.2 nm, suggesting they correspond to fluorine sites, whereas with longer wavelengths

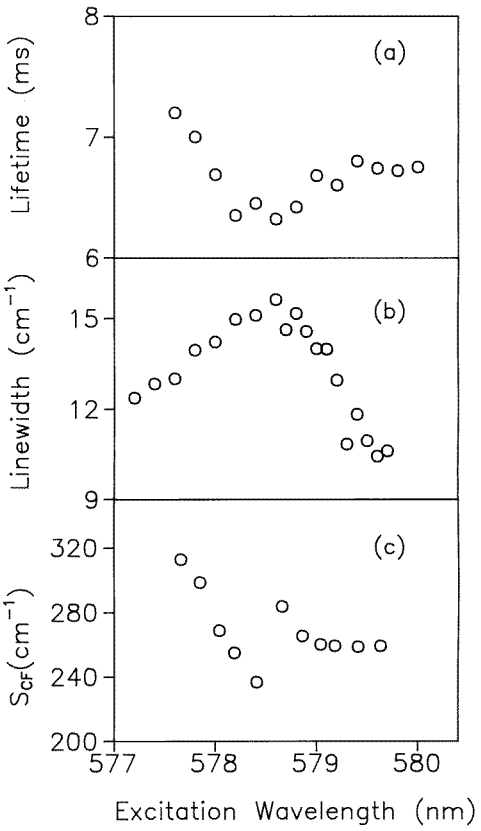

Figure 12. (a) Lifetime of the $^5D_0 \rightarrow {}^7F_2$ transition, (b) linewidth of the time-resolved resonant line-narrowed $^5D_0 \rightarrow {}^7F_0$ emission and (c) crystal field strength of CNBZn glass doped with 0.5 mol% of Eu^{3+} as a function of excitation wavelength along the $^7F_0 \rightarrow {}^5D_0$ absorption band. Data correspond to 4.2 K.

the hypersensitive $^5D_0 \rightarrow {}^7F_2$ transition clearly shows a different shape (for CNBZn glass), which might be due to the influence of chlorine ions. Further arguments about the chlorine influence on the spectroscopic behaviour of europium in CNBZn glass will be given in the next section.

4.2.3. Estimation of the crystal field strength. The $^5D_0 \rightarrow {}^7F_1$ transition of Eu^{3+} ion is a parity-allowed magnetic dipole transition and its strength does not vary significantly with the crystal field acting on the ion. Therefore the influence of glass composition on the site-selective excited emission spectra of Eu^{3+} can be described by the ratio of the $^5D_0 \rightarrow {}^7F_2$ and $^5D_0 \rightarrow {}^7F_1$ emission intensities which is related to the Judd–Ofelt parameter Ω_2. This parameter is related in turn to the covalency and/or structural changes in the vicinity of Eu^{3+} ions [51]. Though a more covalent bonding character would be expected for the mixed fluorochloride glass, figure 13 shows that the ratio of the $(^5D_0 \rightarrow {}^7F_2)/(^5D_0 \rightarrow {}^7F_1)$ intensities is lower for CNBZn glass than for pure fluoride glass, which points to a higher symmetry for Eu^{3+} ion sites. As C_{2v} local symmetry is the highest one allowing full splitting of the $^7F_1$ and $^7F_2$ levels of Eu^{3+}, and with account taken of the above-mentioned results, it was chosen as the most appropriate symmetry for the crystal field analysis of site-selective

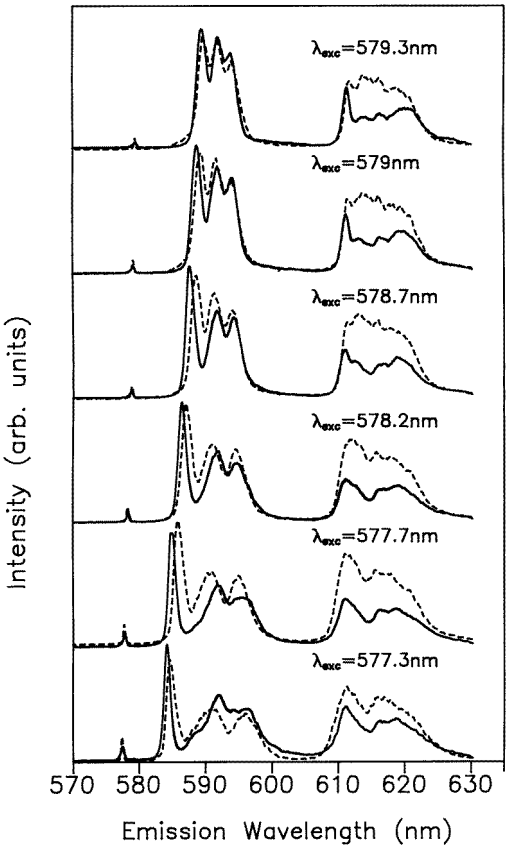

Figure 13. Time-resolved line-narrowed emission spectra of $^5D_0 \rightarrow {}^7F_{0,1,2}$ transitions of Eu^{3+} ions in CNBZn glass (solid line) and in BIGaZYTZr glass (dashed line) doped with 0.5 mol% of Eu^{3+} ions. The fluorescence was measured at 4.2 K at a time delay of 1 ms after the laser pulse and at different excitation wavelengths.

spectra of Eu^{3+} in CNBZn glass.

Crystal field calculations were carried out by using the single-particle crystal field theory [52, 53]. In Wybourne's formalism the crystal field Hamiltonian is expressed as a sum of products of spherical harmonics and crystal field parameters:

$$H_{CF} = \sum_{k=2}^{4,6} \sum_{q=0}^{k} [B_q^k (C_q^k + (-1)^q C_{-q}^k) + \mathrm{i} S_q^k (C_q^k - (-1)^q C_{-q}^k)]. \tag{7}$$

The number of nonzero crystal field parameters B_q^k depends on the point-site symmetry of the rare-earth ion.

The B_q^k associated with the C_{2v} point symmetry are $B_0^2,\ B_2^2,\ B_0^4,\ B_2^4,\ B_4^4,\ B_0^6,\ B_2^6,\ B_4^6$ and B_6^6 (for C_{2v} symmetry all S_q^k in the above Hamiltonian vanish). As the $^5D_0 \rightarrow {}^7F_J$ transitions for $J > 2$ were not resolved and showed no significant excitation-dependent spectral changes, we made no attempt to include such levels in our calculations. Nevertheless, as we shall see, the calculated $B_q^{2,4}$ crystal field parameters give enough evidence about the different bond strengths at the fluorinelike and chlorinelike sites. The procedure consists of a two-step calculation. The first one finds the B_q^2 sets simulating the

$^7F_1$ splitting, whereas the second one keeps B_q^2 fixed and includes the fourth-order crystal field parameters B_q^4 and experimental $^7F_2$ levels in order to test the possible values and to choose the best B_q^4 set from the smallest rms deviation. All the simulations were performed by the FORTRAN computer program GROMINET [54]. Table 5 includes the results for the calculated B_q^k.

Table 5. Observed crystal field parameters as a function of excitation energy along the $^7F_0 \rightarrow {}^5D_0$ transition for Eu^{3+} in CNBZn glass.

Excitation energy (cm^{-1})	B_0^2	B_2^2	B_0^4	B_2^4	B_4^4
17 311.22	−955.78	227.59	529.27	−235.55	457.22
17 305.52	−835.98	218.82	889.49	−347.07	230.5
17 299.84	−831.09	215.25	459.17	−306.07	265.17
17 295.35	−770.45	212.17	479.11	−290.4	249.83
17 288.77	−722.77	210.35	467.13	−8.39	311.09
17 281.30	−598	167.55	871.33	−488.85	310.24
17 275.33	−520.43	150.81	840.43	−500.94	247.98
17 269.96	−454.34	139.39	811.59	−579.52	165
17 265.78	−414.27	125.36	815.44	−605.5	158.48
17 258.93	−357.84	118.85	810.39	−635.64	172.46
17 252.38	−291.27	100.53	850.71	−649.46	167.06

As we were mainly interested in the investigation of the effects of the ligand anion on the radiative transition rate of the rare earth, which obviously depends on the symmetry of the site, we have used the average strength S_{CF} of the crystal field acting on the Eu^{3+} ions defined in the following way [55]:

$$S_{CF} = \left\{ \frac{1}{3} \sum_k \frac{1}{(2k+1)} \left[(B_0^k)^2 + 2 \sum_{q>0} (B_q^k)^2 \right] \right\}^{\frac{1}{2}}. \tag{8}$$

Figure 12(c) shows the variation of the S_{CF} values as a function of the selective $^7F_0 \rightarrow {}^5D_0$ excitation wavelength within the inhomogeneous band profile. The spectral features show a nonuniform behaviour of the S_{CF} strength at the different rare-earth sites analogous to the behaviour of the lifetimes.

A plausible model proposed to explain the nonmonotonic behaviour of the lifetimes, narrowed linewidths and S_{CF} strengths as a function of excitation wavelength could be based on the incorporation of chlorine ions to the nearest-neighbour coordination of the Eu^{3+} ion giving more distorted local environments. With the addition of chlorine ions, some of the fluorine first-neighbour coordination ions may be replaced. With account taken of the different electronegativity and atomic radii of both ions, the incorporation of chlorine will produce two effects: (i) some weakening of the crystal field strength and (ii) a lowering of the rare-earth site symmetry. This symmetry distortion will enhance the $^5D_0 \rightarrow {}^7F_2$ electric dipolar transition rate and produce the observed decrease in the lifetimes as excitation wavelength increases (figure 12(a)). The distortion may also enhance the homogeneous linewidths which are dominated by relaxation time broadening caused by rapid phonon relaxation processes. This situation will come to an end when the first coordination shell of Eu^{3+} ions is stabilized as far as chlorine ions are concerned. For these sites, we can expect some increase of lifetimes and a decrease of crystal field and homogeneous linewidths as excitation wavelength increases [15] (as is experimentally observed). In any

case, this nonmonotonic behaviour of lifetimes, narrowed linewidths and S_{CF} strengths as a function of excitation wavelength suggests the existence of some site segregation for the rare earth in these mixed fluorochloride glasses. Finally, these results show the high sensitivity of fluorescence line-narrowing spectroscopy as a local order probing tool in glasses.

One of the difficulties in further exploring the local average structure around the Eu^{3+} ion in CNBZn glass and therefore in validating the interpretation of our experimetal findings is the lack of a structural model for this glass which is composed of six different atoms. As we mentioned in the introduction, there is only a work [27] on MD simulation of Eu^{3+}-doped chlorofluorozirconate glasses which could be of some relevance for the present study. Although the Cd^{2+} ion has a little more electronegativity (1.69 Pauling) than Zr^{4+} (1.33 Pauling), their electronic structure and ionic radii are similar. Therefore, disregarding the influence of Zn^{2+} ions which enter the glass structure as ZnF_2 up to a 10% molar concentration, we could assume, with the corresponding caution, the following conclusions by Takahashi *et al* [27]:

(i) Cl^- substitued for F^- exists around Eu^{3+}, and Cl^- coordination numbers around Eu^{3+} increase in proportion to the Cl^- concentration.

(ii) The total anion coordination number around Eu^{3+} is independent of the Cl^- concentration. In other words, The F^- coordination number decreases with increasing Cl^- coordination number.

(iii) The existence of Cl^- produces the high energy (high frequency) phonon modes around Eu^{3+}.

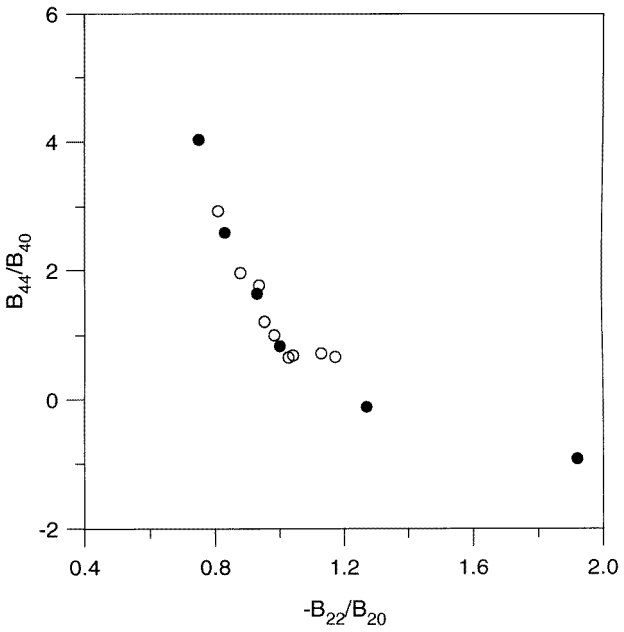

Figure 14. Behaviour of the major crystal-field ratios $-B_{22}/B_{20}$ and B_{44}/B_{40}. The symbols (●) represent values calculated from the geometrical model of Brecher and Riseberg [13]. The symbols (○) indicate the experimental values for CNBZn glass.

Referring to conclusions (i) and (ii), we should stress that the distribution of F^-

coordination numbers in the first coordination shell of Eu^{3+} is very wide, ranging from two to nine, for a substitution of F^- by Cl^- up to 10% in total number of anions whereas the Cl^- coordination number ranges from zero to five for the same composition. The constancy of the coordination number around the rare earth, together with conclusions (i) and (ii), are in agreement with the interpretation of the experimental data that we have presented above. The incorporation of Cl^- to the first coordination shell of Eu^{3+} provides not only a relative softening of the crystal field strength, as is experimentally observed, but also contributes to distort the anion symmetry around the rare earth and therefore promotes an enhancement of the transition rates. Moreover, the appearance of high energy phonon modes associated with the Cl^- incorporation, conclusion (iii), could also explain the decrease in the lifetimes and consequently the increase in the homogeneous linewidths which are dominated by lifetime broadening caused by rapid phonon relaxation processes.

Due to the narrow range of FLN experimental data available for CNBZn glass, it is difficult to generate a geometrical model for the environment of the europium ion which could be taken as the starting point for a theoretical calculation of the crystal field parameters. However, we have made an attempt to compare the ratios of the crystal field parameters $-B_{22}/B_{20}$ and B_{44}/B_{40} (carrying the pure orientational information about the coordination) calculated from our experimental data with those following a model for the average structure of the Eu^{3+} sites in a glassy host developed by Brecher and Riseberg [13] and later applied by other authors [19]. The model involves eight approximately equidistant oxygen anions in a geometrical arrangement of a slightly elongated Archimedean antiprism with C_{2v} symmetry with a ninth coordinator which may continuously shift its position along the twofold symmetry axis approaching a final position which gives a ninefold coordination. The assumption that Eu^{3+} is eightfold or ninefold coordinated in CNBZn glass is consistent with the above mentioned MD simulation results [27]. For the excitation range shown in table 5 the relative changes in magnitude of both B_{22}/B_{20} and B_{44}/B_{40} ratios agree fairly well with the theoretical ratios by Brecher and Riseberg. As the excitation wavelength goes from high to low energies, the value of B_{22}/B_{20} increases by around 25% whereas the B_{44}/B_{40} ratio decreases by a factor of four. However, the values of our ratios should be corrected by a factor of 3.4 in order to attain the theoretical values of Brecher and Riseberg. The lowering of our values could be related, as already mentioned by Capobianco *et al* [19] to the sensitivity of the crystal field parameter B_{20} to the magnitude of the electrostatic interactions. In our case, an increase of B_{20} and B_{40} could be expected, if account is taken of the difference in the degree of covalency between metal–oxygen and metal–fluorine or chlorine bonds. Figure 14 shows a plot of the theoretical ratios $-B_{22}/B_{20}$ and B_{44}/B_{40} by Brecher and Riseberg and those calculated for CNBZn glass multiplied by a factor of 3.4. As can be seen the ratios for CNBZn follow the theoretical ones up to an excitation wavelength close to 579 nm at which a sharp change occurs. This wavelength region coincides with the one in which a nonuniform behaviour in the decays and linewidths of the line-narrowed fluorescence occurs and seems to confirm the existence of europium environments where the presence of Cl^- begins to dominate the local coordination around the europium ion.

5. Conclusions

From the above results the following conclusions can be reached.

(i) The presence of chlorine ions in CNBZn glass results in higher values for the JO parameters, narrower effective linewidth and larger value for the $^4F_{3/2} \rightarrow {}^4I_{11/2}$ stimulated

emission cross-section as compared with pure fluoride glasses.

(ii) The nonradiative Nd–Nd relaxation rates of the $^4F_{3/2} \rightarrow {}^4I_{11/2}$ transition were found to increase with temperature as T^3 in the 10–90 K temperature range for concentrations higher than 0.5 mol%. This behaviour, also found in pure fluoride matrices, is in agreement with a two-site nonresonant process.

(iii) The quantum efficiency of the $^4F_{3/2} \rightarrow {}^4I_{11/2}$ emission of Nd^{3+} in fluorochloride glass is higher than in pure fluoride glasses.

(iv) Time-resolved emission spectra of the $^4F_{3/2} \rightarrow {}^4I_{11/2}$ emission for fluorochloride glass doped with 1 mol% of Nd^{3+} show the presence of energy transfer among Nd^{3+} ions. However, the transfer is fast enough to give exponential fluorescence decays.

(v) The results of site-selective laser spectroscopy show that in spite of the high fluoride content of CNBZn glass, the presence of chlorine ions greatly affect the local environment at the Nd^{3+} site. In particular, the excitation wavelength dependence of the $^4F_{3/2}$ lifetimes points to the existence of some site segregation for Nd^{3+} ions in this fluorochloride glass, and suggests the presence of different kinds of ion in the first coordination shell of the rare earth.

(vi) FLN experiments performed with Eu^{3+} ions in the same glass confirm the presence of different kinds of coordination ion. The nonuniform behaviour shown by the average strength of the crystal field acting on the Eu^{3+} ions, by the decays of the line-narrowed fluorescence of the $^5D_0 \rightarrow {}^7F_2$ hypersensitive transition and by the homogeneous linewidth of the $^5D_0 \rightarrow {}^7F_0$ transition, as a function of the selective $^7F_0 \rightarrow {}^5D_0$ excitation wavelength, might be interpreted as indicating a crossover between the behaviour of fluorinelike and chlorinelike coordination anions.

Acknowledgments

This work was supported by the Basque Country University (EB034/95), by the Spanish Government (Acciones Integradas HF-218B, HF-0205 and DGICYT PB95-0512), and Basque Country Government (PI95/88).

References

[1] Weber M J 1982 *J. Non-Cryst. Solids* **47** 117
[2] Eckersley M C, Gaskell P H, Barnes A C and Chieux P 1988 *Nature* **335** 525
[3] Lucas J and Adam J L 1989 *Glastech. Ber.* **62** 422 and references therein
[4] van Uiter L G and Wemple S H 1978 *Appl. Phys. Lett.* **33** 57
[5] Angell C A, Changh L and Sundar H G K 1985 *Mater. Sci. Forum* **5** 189
[6] Matecki M, Poulain M and Poulain M 1987 *Mater. Sci. Forum* **19/20** 47
[7] Adam J L, Matecki M, L'Helgoualch H and Jaquier B 1994 *Eur. J. Solid State Inorg. Chem.* **31** 337
[8] Weber M J 1990 *J. Non-Cryst. Solids* **123** 208
[9] Stokowski S E 1987 *Laser, Spectroscopy and New Ideas* (Berlin: Springer)
[10] Weber M J 1981 *Laser Spectroscopy of Solids* (Berlin: Springer)
[11] Yen W M 1986 *Optical Spectroscopy of Glasses* (Dordrecht: Reidel)
[12] Motegi N and Shionoya S 1973 *J. Lumin.* **8** 1
[13] Brecher C and Riseberg L A 1976 *Phys. Rev.* B **13** 81
[14] Hegarty J, Yen W M and Weber M J 1978 *Phys. Rev.* B **18** 5816
[15] Brecher C and Riseberg L A 1980 *Phys. Rev.* B **21** 2607
[16] Gang Xu, Boulon G and Powell R C 1983 *J. Chem. Phys.* **78** 4374
[17] Gang Xu and Powell R C 1985 *J. Appl. Phys. 57* 1299
[18] Nishimura G and Kushida T 1988 *Phys. Rev.* B **37** 9075
[19] Capobianco J A, Proulx P P, Bettinelli M and Negrisolo F 1990 *Phys. Rev.* B **42** 5936
[20] Balda R, Fernández J, Eilers H and Yen W M 1994 *J. Lumin.* **59** 81

[21] Pucker G, Gatterer K, Fritzer H P, Bettinelli M and Ferrari M 1996 *Phys. Rev.* B **53** 6225
[22] Balda R, Fernández J, Adam J L and Arriandiaga M A 1996 *Phys. Rev.* B **54** 12 076
[23] Cormier G, Capobianco J A and Monteil A 1993 *J. Non-Cryst. Solids* **152** 225
[24] Cormier G, Capobianco J A, Morrison C A and Monteil A 1993 *Phys. Rev.* B **48** 16 290
[25] Adam J L, Ponçon V, Lucas J and Boulon G 1987 *J. Non-Cryst. Solids* **91** 191
[26] Durville F, Dixon G S and Powell R C 1987 *J. Lumin.* **36** 221
[27] Takahashi M, Yamamoto R, Kano R and Kawamoto Y 1995 *J. Phys.: Condens. Matter* **7** 4583
[28] Judd B R 1962 *Phys. Rev.* **127** 750
[29] Ofelt G S 1962 *J. Chem. Phys.* **377** 511
[30] Krupke W F 1974 *IEEE J. Quantum Electron.* **QE-10** 450
[31] Carnall W T, Crosswhite H and Crosswhite H M 1977 *Argonne National Laboratory Report*
[32] Balda R, Fernández J, Mendioroz A, Adam J L and Boulard B 1994 *J. Phys.: Condens. Matter* **6** 913
[33] Jacobs R R and Weber M J 1976 *IEEE J. Quantum Electron.* **QE-12** 102
[34] Reisfeld R and Jorgensen C K 1977 *Lasers and Excited States of Rare Earths* (Berlin: Springer)
[35] Brecher C, Riseberg L A and Weber M J 1978 *Phys. Rev.* B **18** 5799
[36] Tesar A, Campbell J, Weber M, Weinzapfel C, Lin Y, Meissner H and Toratani H 1992 *Opt. Mater.* **1** 217
[37] Jørgensen C K and Reisfeld R 1983 *J. Less-Common Met.* **93** 107
[38] Weber M J, Ziegler D C and Angell C A 1982 *J. Appl. Phys.* **53** 4344
[39] Holstein T, Lyo S K and Orbach R 1981 *Laser Spectroscopy of Solids* (Berlin: Springer)
[40] Balda R, Fernández J, de Pablos A and Fdez-Navarro J M 1996 *Phys. Rev.* B **53** 5181
[41] Elejalde M J, Balda R, Fernández J, Macho E, Adam J L and Lucas J 1992 *Phys. Rev.* B **46** 5169
[42] Weber M J 1971 *Phys. Rev.* B **4** 2932
[43] Balda R, Fernández J, Illarramendi M A, Arriandiaga M A, Adam J L and Lucas J 1991 *Phys. Rev.* B **44** 4759
[44] Illarramendi M A, Fernández J, Balda R, Lucas J and Adam J L 1991 *J. Lumin.* **47** 207
[45] Balda R, Fernández J, Elejalde M J, Illarramendi M A and Jacoboni C 1991 *J. Phys.: Condens. Matter* **3** 7695
[46] Azkargorta J, Iparraguirre I, Balda R, Fernández J, Dénoue E and Adam J L 1994 *IEEE J. Quantum Electron.* **30** 1862
[47] Azkargorta J, Iparraguirre I, Balda R, Fernández J, Adam J L, Dénoue E and Lucas J 1997 *J. Non-Cryst. Solids* **213/214** 271
[48] Selzer P M 1981 *Laser Spectroscopy of Solids* (Berlin: Springer)
[49] Jorgensen C K and Judd B R 1964 *Mol. Phys.* **8** 291
[50] Reisfeld R and Jorgensen C K 1977 *Lasers and Excited States of Rare Earths* (Berlin: Springer)
[51] Oomen E W J L and van Dongen A M A 1989 *J. Non-Cryst. Solids* **111** 205
[52] Wybourne B G 1965 *Spectroscopic Properties of Rare Earths* (New York: Wiley)
[53] Hüfner S 1968 *Optical Spectra of Transparent Rare Earth Compounds* (New York: Academic)
[54] Porcher P 1995 Fortran routine GROMINET for simulation of real and complex crystal field parameters on $4f^6$ and $4f^8$ and configurations (unpublished)
[55] Chang N C, Gruber J B, Leavitt R P and Morrison C A 1982 *J. Chem. Phys.* **78** 3877